1

Morphological study of embryonic *Chd8+/-* mouse brains using light-sheet microscopy

Authors:

Harold F. Gómez[1,2#], Leonie Hodel[1#], Odyssé Michos[1,2], and Dagmar Iber[1,2*],

Affiliations:

[1] Department of Biosystems, Science and Engineering (D-BSSE), ETH Zurich, Mattenstraße 26, 4058 Basel, Switzerland

[2] Swiss Institute of Bioinformatics (SIB), Mattenstraße 26, 4058 Basel, Switzerland

[#] These authors contributed equally.

[*] Corresponding authors.

Correspondences:

Harold F. Gómez: harold.gomez@bsse.ethz.ch

Leonie Hodel: leonie.hodel@gess.ethz.ch

Odyssé Michos: odysse.michos@gmail.com

Dagmar Iber: dagmar.iber@bsse.ethz.ch

2

Abstract

Objective

Autism spectrum disorder (ASD) encompasses a group of neurodevelopmental conditions that remain poorly understood due to their genetic complexity. *CHD8* is a risk allele strongly associated with ASD, and heterozygous *Chd8* loss-of-function mice have been reported to exhibit macrocephaly in early postnatal stages. In this work, we sought to identify measurable brain alterations in early embryonic development.

Results

We performed light-sheet fluorescence microscopy imaging of N-cadherin stained and optically cleared *Chd8*$^{+/-}$ and wild-type mouse brains at embryonic day 12.5 (E12.5). We report a detailed morphometric characterization of embryonic brain shapes and cortical neuroepithelial apical architecture. While *Chd8*$^{+/-}$ characteristic expansion of the forebrain and midbrain was not observed this early in embryogenesis, a tendency for a decreased lateral ventricular sphericity and an increased intraocular distance in *Chd8*$^{+/-}$ brains was found compared to controls. This study advocates the use of high-resolution microscopy technologies and multi-scale morphometric analyses of target brain regions to explore the etiology and cellular basis of *Chd8* haploinsufficiency.

Keywords

Light-sheet microscopy, Chd8, Mouse brains, Autism, Tissue clearing, Morphometry, Lewis' Law, Aboav-Weaire's Law.

3

Introduction

46

47   Autism spectrum disorder (ASD) is a poorly understood disease due to significant genetic complexity and

48   phenotypic heterogeneity. Despite our improved understanding of how ASD develops (1–5), mapping the

49   relative contribution of risk alleles to neuroanatomical abnormalities and clinically observed phenotypes like

50   macrocephaly remains challenging.

51   Genetic studies have implicated mutations in more than 800 genes of diverse function in the etiology of

52   ASD (1). One of the most strongly associated genes is the chromodomain helicase DNA-binding protein 8

53   *CHD8*, an ATP-dependent chromatin remodeler, and transcriptional repressor. Patients with loss-of-

54   function (LOF) mutations in *CHD8* exhibit gene haploinsufficiency, display altered behavior, and region-

55   specific anomalies in brain morphology and physiology that manifest during early childhood (6–8). Similarly,

56   *Chd8* haploinsufficiency in mice results in neonatal macrocephaly, increased brain weight, and craniofacial

57   abnormalities (9–11), mirroring clinical observations in patients and suggesting similar developmental

58   trajectories between species.

59   ASDs are largely hypothesized to originate in utero from profound perturbations in neural stem cell niche

60   regions of the developing brain (12). Gene expression profiling in the embryonic mouse cortex of *Chd8*

61   haploinsufficient mice shows a temporal modulation of *Chd8* that peaks at E12, and helps negotiate the

62   complex balance between neuronal expansion (prior to E12.5) and differentiation (E12.5 to postnatal) (13).

63   As a result, dysregulations of *Chd8* dynamics during embryonic cortical development in mice prematurely

64   deplete the neural progenitor pool, consistent with a lower density of neural cells and metabolic components

65   observed in children with ASD (14). In spite of novel neurodevelopmental evidence, it is unknown whether

66   these in utero perturbations manifest as distinctive anatomical dysmorphologies before the postnatal onset

67   of characteristic ASD phenotypes (15).

68   In this study, we investigated the morphological consequences of *Chd8* haploinsufficiency during embryonic

69   mouse brains at the whole-organ and cellular level. To anticipate anatomical findings in a condition with

70   early-life onset, we leveraged N-cadherin staining, light-sheet fluorescence microscopy, and CUBIC tissue

71   clearing (16) to examine the neuroanatomical differences between E12.5 mouse brains with germline *Chd8*$^{+/-}$

72   LOF mutations (10) and litter-matched wild-types. We report slight differences in intraocular distance and

4

73 ventricular sphericity and introduce a detailed approach for comparing cortical neuroepithelial apical

74 architecture. Taken together, these datasets provide a new avenue for querying the developmental role of

75 *CHD8* and the cellular remodeling that is likely to precede associated post-birth brain malformations in

76 haploinsufficiency cases.

77

Methods and materials

Animals

80 Mice with loss-of-function mutations in *Chd8* were generated using Cas9-mediated germline editing (10).

Immunofluorescence on embryonic brains

82 Following dissection, all E12.5 mouse brains were fixed with 4% paraformaldehyde in PBS. Samples were

83 then incubated with anti-N-cadherin antibody (BD Transduction Laboratories; Material No. 610920; 1:200)

84 at 4 °C for 3 days. After washing in D-PBS, brains were incubated with conjugated fluorescent secondary

85 Alexa Fluor 555 donkey anti-mouse IgG (H+L) (Abcam; Material No. ab150106; 1:250) for 2 days at 4 °C.

Optical clearing and light-sheet imaging

87 Whole-mount clearing was performed with the Clear Unobstructed Brain/Body Imaging Cocktails and

88 Computational Analysis (CUBIC) protocol (16). Delipidation and refractive index matching were carried

89 out with reagent-1 [25% (w/w) urea, 25% ethylenediamine, 15% (w/w) Triton X-100 in distilled water] and

90 reagent-2 [25% (w/w) urea, 50% (w/w) sucrose, 10% (w/w) nitrilotriethanol in distilled water], respectively.

91 Samples were incubated in 1/2 reagent-1 (CUBIC-1:H2O=1:1) for 1 day and then in 1X reagent-1 until

92 transparent. All samples were washed several times in PBS and treated with 1/2 reagent-2 (CUBIC-

93 2:PBS=1:1) for around 3 days. Lastly, incubation in 1X reagent-2 was done until transparency was achieved,

94 and the solution became homogeneous. All steps were performed on a shaker at room temperature.

95 Fluorescence images were acquired using a Zeiss Lightsheet Z.1 microscope. Acquisition optics included a

96 Zeiss 20x/1.0 Plan Apochromat water-immersion objective to acquire cell resolution data, and a Zeiss

97 5x/0.1 air objective lens for larger fields of view (whole brains). All image stacks were deconvolved using

5

98 Huygens deconvolution to improve contrast and resolution and further pre-processed in Fiji (17) to

99 accentuate feature boundaries.

3D surface reconstruction of whole mouse brains

101 3D segmentation of the embryonic ventricles and cerebral cortex was conducted with Imaris

102 MeasurementPro, a component of Imaris v9.1.2 (BitPlane, South Windsor, CT, USA). This enabled the

103 computational interpolation of planar 2D surface outlines from successive horizontal sections into 3D iso-

104 surface. Contours were drawn on magnified images to allow sub-voxel precision and faithful delineation of

105 small-scale features (Fig. 1). Quantified brain surface features included volume and surface area. Intraocular

106 distance was measured in 3D using measurement points placed in the center of the pupils.

107 As the cortex has broad irregular anatomical features that make absolute cortical thickness measurements

108 challenging, we considered the cortex to be a hollow cylinder with volume V and area A. In this way, the

109 cortical height of the neuroepithelial layer could be approximated as

$$h_{cortex} = \frac{2V_{cortex}}{A_{outer} + A_{inner}}$$

112 Furthermore, to derive ventricular sphericity, lateral ventricle iso-surfaces were separated at the septum

113 pellucidum. The sphericity of each 3D entity was then determined as

$$S_{ventr} = \frac{\pi^{\frac{1}{3}}(6V_{ventr})^{\frac{2}{3}}}{A_{ventr}}$$

Morphometric measurements of apical neuroepithelia

117 Cell morphology in the apical layer of the cortical epidermis was investigated using the open-source software

118 platform MorphoGraphX (18). A curved 2.5D image projection was constructed by meshing the apical

119 boundary and projecting 2-6 μm of the most apical signal onto it. Then, the Watershed algorithm was used

120 to segment all cell boundaries, some of which required manual curation. All border cells were excluded from

121 the analysis.

122 To characterize all projected polygonal apical lattices, quantifications on cellular areas and neighbour

123 numbers were imported into the R software platform. Apical packing was also explored via known

6

124   regularities of epithelial lattices. Termed Lewis' Law, this property linearly relates the measured average cell

125   area $\bar{A}$ and neighbour number n and has been previously described in all apical epithelia studied to date

126   (19,20).

127

$$\frac{\bar{A}_n}{\bar{A}} = \frac{(n-2)}{4}$$

128   As cells with small polygon numbers have the tendency to be in contact with cells of larger polygon numbers

129   and vice-versa, one also observes that the average number of neighbours of all n cells that border a cell with

130   n neighbours follows

131

$$m(n) = 5 - \frac{n}{8}$$

132   a relationship termed Aboav-Weaire's Law (21,22). Lastly, the cell aspect ratio was calculated using an in-

133   house algorithm that leverages MorphoGraphX's modularity to fit an ellipse and extract major and minor

134   axes for each cell outline.

135

136   **Results**

137   **ASD-associated craniofacial phenotypes in Chd8^{+/-} mice**

138   To determine whether *Chd8* heterozygous mice exhibit structural and craniofacial ASD phenotypes during

139   embryonic development, we tested for differences in brain morphology between E12.5 *Chd8^{+/-}* and control

140   animals. To this extent, user-assisted 3D segmentation software tools were used to derive iso-surface

141   representations from volumetric image stacks and enable tissue quantification measures of size, shape, and

142   asymmetry (Fig. 1).

143   We then characterized different anatomical features in both cortical and ventricular regions to reveal regional

144   alterations (Fig. 2). Overall brain volume, including ventricles, showed no significant difference between the

145   two groups (wild-type [n=2] 3.41 mm³ and 3.15 mm³, *Chd8^{+/-}* [n=5] 3.60 ± 0.56 mm³) (Fig. 2a). Similarly,

146   measured cortical volumes excluding the ventricular space showed no difference (wild-type [n=2] 2.17 mm³

147   and 2.15 mm³, *Chd8^{+/-}* [n=5]: 2.47 ± 0.37 mm³). Individual ventricular volume was consistent within and

148   between groups (wild-type [n=4] 0.56 ± 0.07 mm³, *Chd8^{+/-}* [n=10] 0.57 ± 0.14 mm³). Furthermore, we

149   observed no differences in brain surface area (wild-type [n=2] 15.6 mm² and 14.5 mm², $Chd8^{+/-}$ [n=5] 15.48

150   ± 1.63 mm²) or in ventricular surface area (wild-type [n=4] 4.66 ± 0.30 mm², $Chd8^{+/-}$ [n=10] 4.95 ± 0.83

151   mm²) between $Chd8^{+/-}$ and wild-type littermates (Fig. 2b).

152   *CHD8* mutant patients often present craniofacial abnormalities (7). We report a slight increase in the

153   intraocular distance and variability within the $Chd8^{+/-}$ group (wild-type [n=2] 1.75 ± 0.002 mm, $Chd8^{+/-}$

154   [n=3] 1.85 ± 0.10 mm) (Fig. 2c), which is consistent with mouse studies from similar genetic backgrounds

155   (10). Moreover, we observed a slight decrease in ventricular sphericity in $Chd8^{+/-}$ mice (wild-type [n=4] 0.70

156   ± 0.01, $Chd8^{+/-}$ [n=10] 0.67 ± 0.03) (Fig. 2d). We also found a higher variability in whole-brain cortical

157   thickness in $Chd8^{+/-}$ mice (wild-type [n=2] 0.08 ± 0.02 mm, $Chd8^{+/-}$ [n=5] 0.10 ± 0.03 mm) (Fig. 2e). Thus,

158   only some craniofacial phenotypes were detected during early embryonic development.

159   **Quantifying apical cell morphology in Chd8$^{+/-}$ mice**

160   To identify cellular and tissue mechanics abnormalities preceding ASD-associated macrocephaly, we used

161   MorphoGraphX to isolate and mesh the apical boundaries of imaged epithelial cell patches in matching

162   regions of the cerebral cortex (18). By taking tissue curvature into account, we segmented a large number

163   of cell outlines from one $Chd8^{+/-}$ [n=3854] and one wild-type [n=1031] sample (Fig. 3a-b).

164   Apical organization was quantified by geometrical properties such as cell number of neighbours, areas, and

165   aspect ratio. We found similar hexagon and heptagon frequencies for the heterozygous (wild-type 29%

166   hexagons, 16% heptagons, $Chd8^{+/-}$ 31% hexagons, 20% heptagons) (Fig. 3c). The observed relation between

167   the polygon type of cells n and the average polygon type of their neighbours m_n termed Aboav-Weaire's Law

168   (21,22), recapitulated results in both the *Drosophila* wing disc and chicken neural tube epithelium (23) (Fig.

169   3d). Similarly, we compared area distributions per polygon type and found no significant difference between

170   groups. The average area per polygon type followed a linear dependency in both samples; a relationship

171   termed Lewis' Law (19,20) (Fig. 3e). Moreover, considering local apical curvature, the aspect ratio was

172   determined by fitting an ellipse to each cell outline and extracting the major and minor axes. The aspect

173   ratio distribution of the $Chd8^{+/-}$ cells was minimally wider than the wild type (Fig. 3f).

174

175

Discussion

177   *Chd8* haploinsufficient mice display various ASD-like phenotypes that parallel the clinical signature of

178   individuals with de-novo *CHD8* mutations (10,11,13,24). Consistent with retrospective patient head

179   circumference data, mouse models for *CHD8* haploinsufficiency suggest a postnatal onset of abnormal head

180   growth (10,11). In this study, we queried the neuroanatomy of $Chd8^{+/-}$ and litter-matched E12.5 control

181   mice using light-sheet microscopy to determine whether morphological anomalies in brain and cortical cell

182   shape could preindicate ASD-associated macrocephaly.

183   The results from a number of longitudinal studies of postnatal volumetric brain changes have implicated

184   neuroanatomical abnormalities in cortical thickness, ventricular morphology, cortical overgrowth, and

185   increased cortical surface area in the complex trajectory of brain development in individuals with ASD

186   (6,25–30). Accordingly, our work characterized cortical thickness along with volumetric features to confirm

187   whether analogous morphological alterations were observable in haploinsufficient mouse brains. We note

188   that in this particular instance, no significant discrepancies in cortical thickness, ventricular and cortical

189   volumes, or surface areas between groups could be determined. In line with the heterogeneous nature of

190   ASD, it is reasonable to assume that other brain regions may be affected instead. Notably, we provide

191   experimental evidence of dissimilarities in ventricular sphericity and intraocular distance that mirror known

192   phenotypes in haploinsufficient adult mice (Fig. 2) (10).

193   Similarly, a number of aberrations at the cellular scale have been reported in ASD during the establishment

194   of cortical microarchitecture (26). Consequently, we sought to ascertain differences in the cortical

195   organization between groups as defined by patterns of cell geometric features measured on the apical surface

196   (Fig. 3). Having quantified epithelial morphology according to the cell area, aspect ratio, neighbour topology,

197   and adherence to empirical laws such as Lewis' and Aboav-Weaire's (Fig. 3), our data showed no departure

198   in the cortical organization between haploinsufficient brains and controls, suggesting similar mechanical

199   behaviour (20,22).

200   In this work, we present a multi-scale assessment of the embryonic neuroanatomical implications of *Chd8*

201   haploinsufficiency in mice. We propose that an increased understanding of the identified organ-level

202   differences may shed light on the etiology of hypertrophic brain growth. What is more, our approach opens

203   exciting avenues to investigate the presence of cellular alterations in other implicated brain regions and

204   phenotypic differences across diverse *Chd8* haploinsufficient mouse models, all of which have a wide range

205   of dosage-specific, dimorphic, and behavioural signatures (24,31).

206

Limitations

208   Underscoring the complexity of autism, our results did not show statistically significant differences in overall

209   morphology with the exception of slight deviations in ventricular sphericity and intraocular distance (Fig.

210   2). Furthermore, our study did not identify aberrations in cortical cellular architecture between groups (Fig.

211   3). We acknowledge that as only a small sample size could be studied (wild-type [n=2], and *Chd8*$^{+/-}$ [n=5]),

212   small morphological differences may have been missed due to the lack of statistical power.

213

Abbreviations

215   **ASD:** autism spectrum disorder

216   **CHD8:** chromodomain helicase DNA-binding protein 8

217   **LOF:** loss-of-function

218   **CUBIC:** clear unobstructed brain/body imaging cocktails and computational analysis

219   **WT:** wild type

220   **HET:** heterozygous

10

References

221 **References**

222 1. Abrahams BS, Geschwind DH. Advances in autism genetics: on the threshold of a new neurobiology.

223 Nature Reviews Genetics. 2008 May;9(5):341–55.

224 2. Iossifov I, Ronemus M, Levy D, Wang Z, Hakker I, Rosenbaum J, et al. De novo gene disruptions in

225 children on the autistic spectrum. Neuron. 2012 Apr 26;74(2):285–99.

226 3. O'Roak BJ, Deriziotis P, Lee C, Vives L, Schwartz JJ, Girirajan S, et al. Exome sequencing in sporadic

227 autism spectrum disorders identifies severe *de novo* mutations. Nature Genetics. 2011 Jun;43(6):585–9.

228 4. Parikshak NN, Luo R, Zhang A, Won H, Lowe JK, Chandran V, et al. Integrative Functional Genomic

229 Analyses Implicate Specific Molecular Pathways and Circuits in Autism. Cell. 2013 Nov 21;155(5):1008–21.

230 5. Sanders SJ, Murtha MT, Gupta AR, Murdoch JD, Raubeson MJ, Willsey AJ, et al. De novo mutations

231 revealed by whole-exome sequencing are strongly associated with autism. Nature. 2012 Apr

232 4;485(7397):237–41.

233 6. Courchesne E. Evidence of Brain Overgrowth in the First Year of Life in Autism. JAMA. 2003 Jul

234 16;290(3):337.

235 7. Bernier R, Golzio C, Xiong B, Stessman HA, Coe BP, Penn O, et al. Disruptive CHD8 Mutations Define

236 a Subtype of Autism Early in Development. Cell. 2014 Jul;158(2):263–76.

237 8. Xu Q, Liu Y, Wang X, Tan G, Li H, Hulbert SW, et al. Autism-associated CHD8 deficiency impairs axon

238 development and migration of cortical neurons. Molecular Autism. 2018 Dec 19;9(1):65.

239 9. Sugathan A, Biagioli M, Golzio C, Erdin S, Blumenthal I, Manavalan P, et al. CHD8 regulates

240 neurodevelopmental pathways associated with autism spectrum disorder in neural progenitors. Proceedings

241 of the National Academy of Sciences. 2014 Oct 21;111(42):E4468–77.

242 10. Platt RJ, Zhou Y, Slaymaker IM, Shetty AS, Weisbach NR, Kim J-A, et al. Chd8 Mutation Leads to

243 Autistic-like Behaviors and Impaired Striatal Circuits. Cell Reports. 2017 Apr 11;19(2):335–50.

244 11. Katayama Y, Nishiyama M, Shoji H, Ohkawa Y, Kawamura A, Sato T, et al. CHD8 haploinsufficiency

245 results in autistic-like phenotypes in mice. Nature. 2016 Sep;537(7622):675–9.

11

246   12. Corley MJ, Vargas-Maya N, Pang APS, Lum-Jones A, Li D, Khadka V, et al. Epigenetic Delay in the

247   Neurodevelopmental Trajectory of DNA Methylation States in Autism Spectrum Disorders. Front Genet.

248   2019 Oct 1;10:907.

249   13. Durak O, Gao F, Kaeser-Woo YJ, Rueda R, Martorell AJ, Nott A, et al. Chd8 mediates cortical

250   neurogenesis via transcriptional regulation of cell cycle and Wnt signaling. Nature Neuroscience. 2016

251   Nov;19(11):1477–88.

252   14. Dager SR, Friedman SD, Petropoulos H, Shaw DWW. Imaging Evidence for Pathological Brain

253   Development in Autism Spectrum Disorders. In: Autism [Internet]. Totowa, NJ: Humana Press; 2008 [cited

254   2019 Nov 6]. p. 361–79. Available from: http://link.springer.com/10.1007/978-1-60327-489-0_17

255   15. Fein D. The Neuropsychology of Autism. OUP USA; 2011. 559 p.

256   16. Susaki EA, Tainaka K, Perrin D, Yukinaga H, Kuno A, Ueda HR. Advanced CUBIC protocols for

257   whole-brain and whole-body clearing and imaging. Nat Protocols. 2015 Nov;10(11):1709–27.

258   17. Schindelin J, Arganda-Carreras I, Frise E, Kaynig V, Longair M, Pietzsch T, et al. Fiji: an open-source

259   platform for biological-image analysis. Nature Methods. 2012 Jun 28;9(7):676–82.

260   18. Barbier de Reuille P, Routier-Kierzkowska A-L, Kierzkowski D, Bassel GW, Schüpbach T, Tauriello G,

261   et al. MorphoGraphX: A platform for quantifying morphogenesis in 4D. eLife [Internet]. 2015 May 6 [cited

262   2017 Aug 25];4. Available from: http://elifesciences.org/lookup/doi/10.7554/eLife.05864

263   19. Lewis FT. The correlation between cell division and the shapes and sizes of prismatic cells in the

264   epidermis of cucumis. The Anatomical Record. 1928 May;38(3):341–76.

265   20. Kokic M, Iannini A, Villa-Fombuena G, Casares F, Iber D. Minimisation of surface energy drives apical

266   epithelial organisation and gives rise to Lewis' law [Internet]. Biophysics; 2019 Mar [cited 2020 Feb 6].

267   Available from: http://biorxiv.org/lookup/doi/10.1101/590729

268   21. Aboav D. The arrangement of grains in a polycrystal. Metallography. 1970 Dec;3(4):383–90.

269   22. Vetter R, Kokic M, Gómez H, Hodel L, Gjeta B, Iannini A, et al. Aboave-Weaire's law in epithelia results

270   from an angle constraint in contiguous polygonal lattices [Internet]. Biophysics; 2019 Mar [cited 2020 Feb

271   6]. Available from: http://biorxiv.org/lookup/doi/10.1101/591461

272   23. Sánchez-Gutiérrez D, Tozluoglu M, Barry JD, Pascual A, Mao Y, Escudero LM. Fundamental physical

273   cellular constraints drive self-organization of tissues. EMBO J. 2016 Jan 4;35(1):77–88.

274   24. Gompers AL, Su-Feher L, Ellegood J, Copping NA, Riyadh MA, Stradleigh TW, et al. Germline Chd8

275   haploinsufficiency alters brain development in mouse. Nature Neuroscience. 2017 Jun 26;20(8):1062–73.

276   25. Courchesne E, Pierce K, Schumann CM, Redcay E, Buckwalter JA, Kennedy DP, et al. Mapping Early

277   Brain Development in Autism. Neuron. 2007 Oct;56(2):399–413.

278   26. Donovan APA, Basson MA. The neuroanatomy of autism - a developmental perspective. J Anat. 2017

279   Jan;230(1):4–15.

280   27. Bigler ED, Tate DF, Neeley ES, Wolfson LJ, Miller MJ, Rice SA, et al. Temporal Lobe, Autism, and

281   Macrocephaly. American Journal of Neuroradiology. 2003 Nov 1;24(10):2066–76.

282   28. Herbert MR, Ziegler DA, Deutsch CK, O'Brien LM, Lange N, Bakardjiev A, et al. Dissociations of

283   cerebral cortex, subcortical and cerebral white matter volumes in autistic boys. Brain. 2003 May

284   1;126(5):1182–92.

285   29. Hazlett HC, Poe M, Gerig G, Smith RG, Provenzale J, Ross A, et al. Magnetic Resonance Imaging and

286   Head Circumference Study of Brain Size in Autism: Birth Through Age 2 Years. Archives of General

287   Psychiatry. 2005 Dec 1;62(12):1366.

288   30. Hazlett HC, Poe MD, Gerig G, Smith RG, Piven J. Cortical Gray and White Brain Tissue Volume in

289   Adolescents and Adults with Autism. Biological Psychiatry. 2006 Jan;59(1):1–6.

290   31. Jung H, Park H, Choi Y, Kang H, Lee E, Kweon H, et al. Sexually dimorphic behavior, neuronal activity,

291   and gene expression in Chd8-mutant mice. Nature Neuroscience. 2018 Sep;21(9):1218–28.

292

13

Declarations

Ethics approval and consent to participate

All animal experiments conducted in the USA followed Public Health Service (PHS) policy and guidelines on humane care, and the use of laboratory animals was approved by the Massachusetts Institute of Technology Committee for Animal Care (CAC).

Consent for publication

Not applicable.

Availability of data and materials

The datasets used and/or analyzed during the current study are available from the corresponding author on reasonable request.

Competing interests

The authors declare that the research was conducted in the absence of any commercial or financial relationships that could be construed as a potential conflict of interest.

Funding

This work has been supported through an SNF Sinergia grant to DI.

Authors' contributions

The study was designed by DI. Staining was done by OM, clearing and imaging by HG. HG and LH analyzed the data and wrote the manuscript. All authors read and approved the final version of the manuscript.

Acknowledgments

We would like to thank Randall Platt and Ashwin S. Shetty for providing the embryos. Moreover, we acknowledge Richard S. Smith for his expert advice on extending MorphoGraphX to enable aspect ratio quantifications of segmented cell outlines.
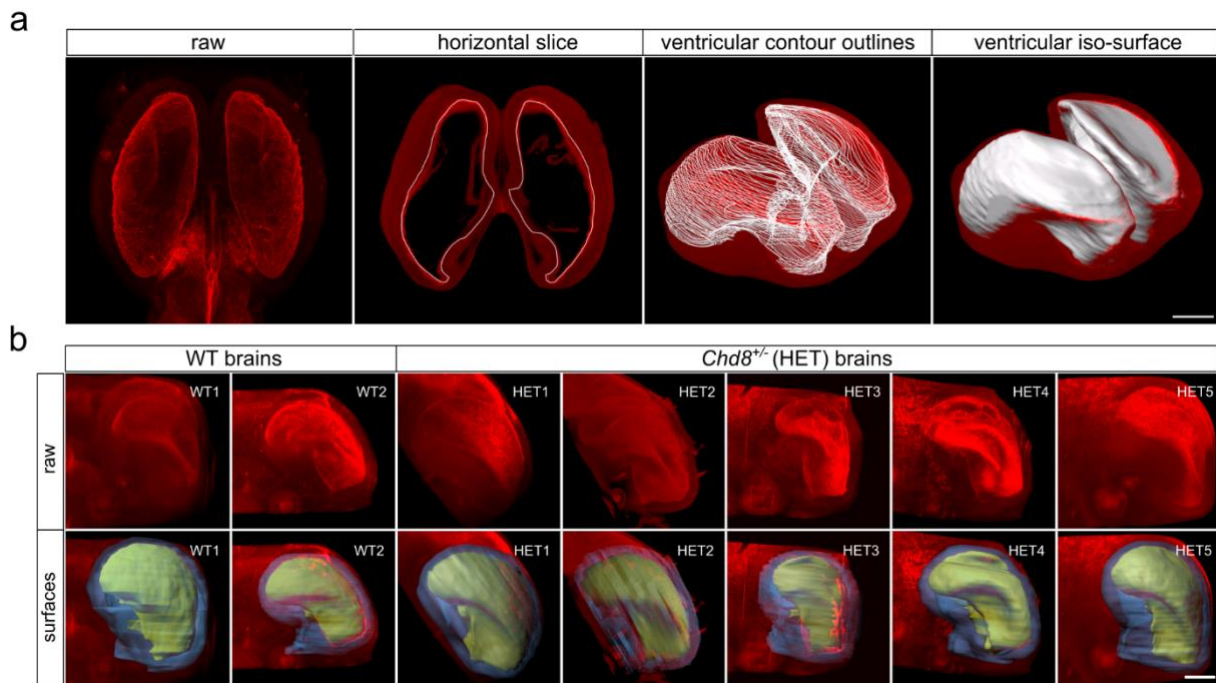
14

Figures and Legends

Figure 1. Volumetric analysis of CUBIC-cleared wild-type and *Chd8*$^{+/-}$ samples, immunostained for N-cadherin (red) to mark neuronal epithelial tissue. **(a)** Illustration of the processing steps in the creation of manual surfaces. Sequential ventricular contours were drawn manually throughout the entire dataset to extract 3D morphology (white outlines). Scale bar 500 μm. **(b)** Raw (top row) and overlays (bottom row) of ventricular (yellow) and cortical (blue) iso-surfaces for each sample. Scale bar 400 μm.
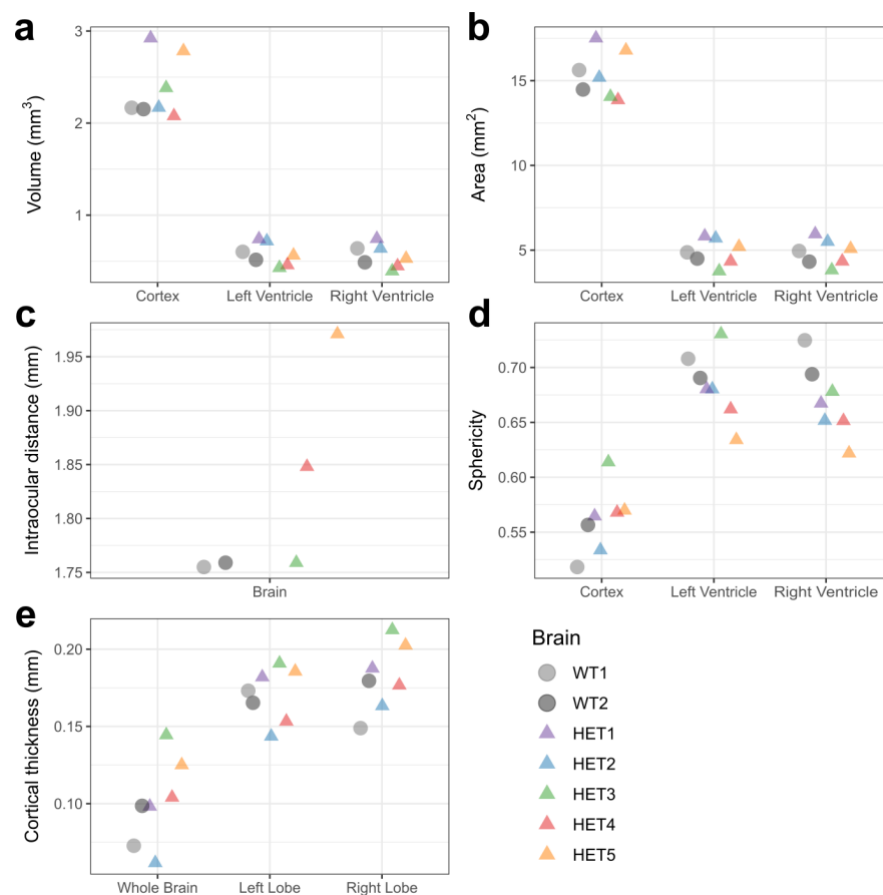
15

Figure 2. Morphological characterization of E12.5 wild-type and *Chd8*^{+/-} mouse brains. **(a-c)** Cortical and ventricular **(a)** volume, **(b)** surface area, and **(c)** intraocular distance. **(d)** Sphericity of cortex and ventricles. **(e)** Cortical thickness of whole brains and left and right lobes. Quantifications were extracted from ventricular and cortical iso-surfaces.
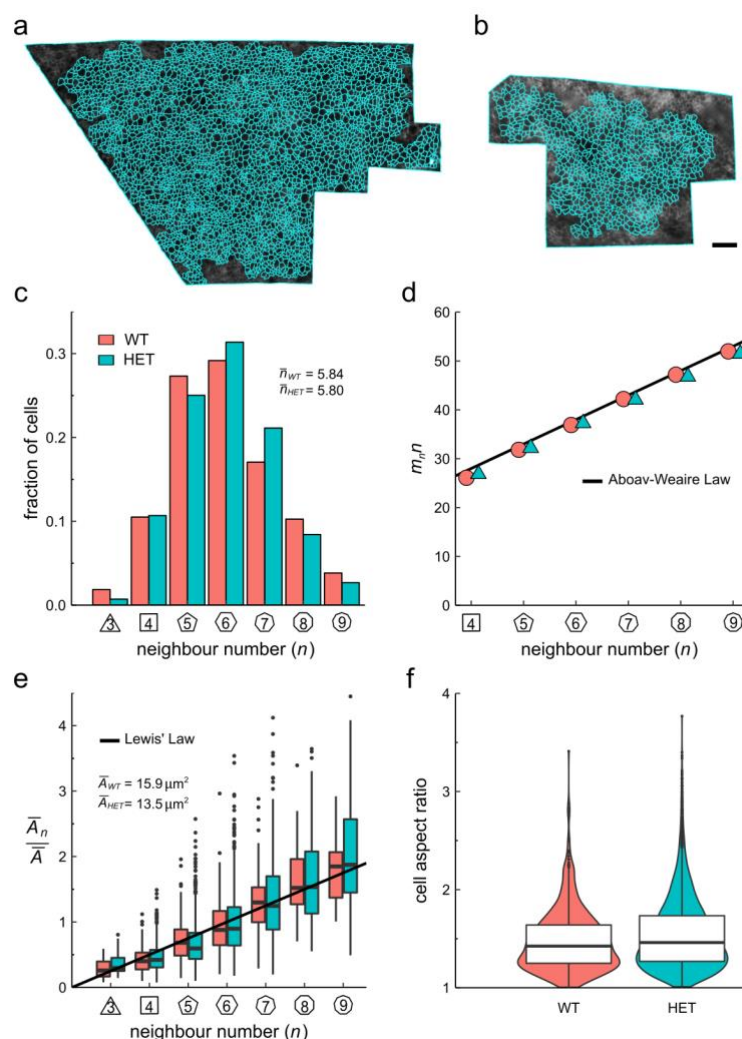
16

Figure 3. Quantification of apical cell morphology in wild-type [n=1031] and *Chd8+/-* [n=3854] E12.5 mouse brains. **(a, b)** 2.5D segmentation overlay of the apical surface of **(a)** *Chd8+/-* (HET) and **(b)** wild-type (WT) neurocortical epithelium. Scale bar: 20 μm. **(c)** Distribution of apical neighbour numbers per sample. The average number of cell neighbours is 5.84 for WT and 5.80 for HET, which is close to the topological requirement of 6. **(d)** Polygon type *n* times the mean polygon number of neighbours *m* of the cell *n* follows a linear relationship termed Aboave-Weaire's Law. **(e)** Average apical cell area by cell neighbour number following a linear relationship termed Lewis' Law (black line). **(f)** Cellular aspect ratios between their longest and shortest axis.